

# Numerical Ricochet Model of a 7.62 mm Projectile Penetrating an Armor Steel Plate

Marvin Becker<sup>1</sup>

Marina Seidl<sup>1</sup>, Jean-François Legendre<sup>1</sup>, Miriam Mehl<sup>2</sup>, M'hamed Souli<sup>3</sup>

<sup>1</sup>French-German Research Institute of Saint-Louis, <sup>2</sup>University of Stuttgart (Institute for Parallel and Distributed Systems), <sup>3</sup>University of Lille (Mechanical Department)

## Abstract

Armored vehicles are designed to favor projectile ricochet and thus avoid perforation while providing a certain surface obliquity for the most probable threat direction. In the latest development not only new materials but also new design approaches are investigated using computer simulations. These simulations allow us to study quantitative dependencies of certain parameters which are difficult to determine experimentally, e.g. the influence of the surface roundness on the ricochet behavior of the projectile.

This paper discusses the ricochet effect of an armor-piercing projectile with hard-core on an armor steel plate. The projectile impacts the target plate with a constant velocity of  $800 \pm 20$  m/s at different oblique angles between  $0^\circ \leq \theta \leq 70^\circ$  (NATO). Besides the residual core velocity ( $v_{res}$ ) which is commonly used for validation purpose, the deflection angle, the detected ballistic limit, which is characterized by the critical angle  $\theta_c$ , and the eroded mass of the target are investigated.

The numerical setup, consists of the explicit Lagrangian LS-DYNA<sup>®</sup> solver, the Johnson-Cook (JC) material and failure model for core and target plus symmetric erosion contact for all parts. Element erosion is provided by the JC-damage model, yet additional core break is neglected.

A good agreement between experiments and simulations of the projectile core was observed, using  $\theta_c$  and  $v_{res}$  as validation parameters in previous studies [1]. In this paper, the model is extended to a fully modeled projectile while defining a lead layer around the core and its brass jacket – both modeled with fully-integrated hexahedral elements and JC-material and damage model. The influence of this modification on the behavior of the projectile core with focus on  $v_{res}$ , deflection angle and eroded mass is discussed in this paper.

## 1. Introduction

In the last decades numerical simulation became a key part in the prototyping for various application. The advantages towards the classical experiments are not only the reduction of manufacturing and test costs, but also reproducibility, expandability to other cases (materials, boundary conditions etc.) and in particular a better insight into the physics where observation techniques are limited.

Thus, on the long run, the goal is to predict arbitrary phenomena with numerical simulation. Unfortunately, achieving this goal contains several challenges and each model contains limitations. In the present investigation of the ricochet behavior of a projectile hitting an armor plate at different oblique angles especially the high pressure, temperature, strain rate and multiaxial load on the material are challenging for the material and fracture model. It is found that the fracture behavior under oblique impact cannot be predicted with existing models in LS-DYNA. Thus, this study focusses on the cases where no failure occurs and investigates the accurateness of the prediction with LS-DYNA.

## 2. Experimental Setup

Experimental investigations are inevitable for validation purpose: a 7.62 mm armor-piercing projectile with a hard-core is penetrating an 8 mm thick inclined plate made of 350 HB armor steel (MARS®190) with a velocity of  $800 \pm 20$  m/s. The experimental setup is depicted in Figure 1: The impact velocity ( $v_0$ ) of the projectile is measured with a light barrier 500 mm in front of the plate, the impact is captured with high speed cameras and x-ray exposure, and the desired oblique angle ( $\theta$ ) can be adjusted with the dedicated device. Unfortunately, the high-speed camera could only be used for determining the straight and stabilized flight of the projectile but not for observing the ricochet effects, since too much dust and fragments obscure the view. The multiple exposed x-ray images are utilized for extracting the residual velocity ( $v_{res}$ ) and the deflection angle ( $\tau$ ).

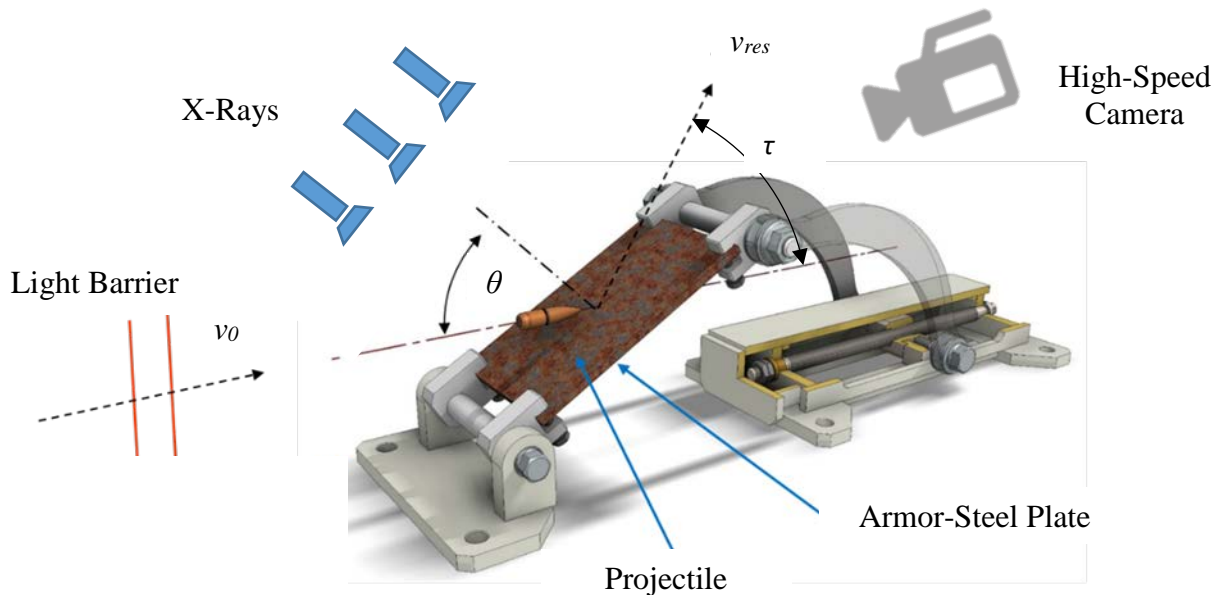


Figure 1: Experimental setup and measurement setup for oblique impact and ricochet investigations.

## 3. Numerical Setup

The generic setup of the oblique impact cases is chosen such that the time from the start of the simulation until the impact remains constant. This means, that the threat needs to be rotated around the point of impact and not around the tip of the projectile. This approach allows to compare the simulation results of different impact scenarios with respect to the elapsed time, which is required since no surjective relation between any physical properties and the displacement can be found for the ricochet cases.

The boundary conditions of the numerical simulation are similar to those of the experiment. To apply the finite element (FE) approach projectile and target have to be discretized with a finite number of elements. Hexahedral elements were chosen due to their smaller stiffness compared to tetrahedral elements.

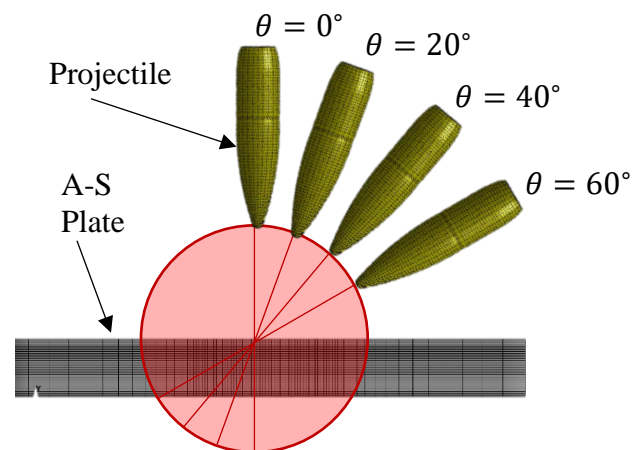
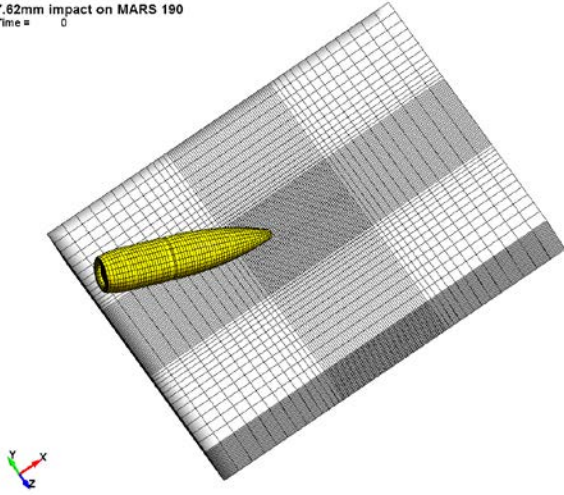


Figure 2: Setup of oblique impact simulation cases.

7.62mm impact on MARS 190  
Time = 0



7.62mm impact on MARS  
Time = 0

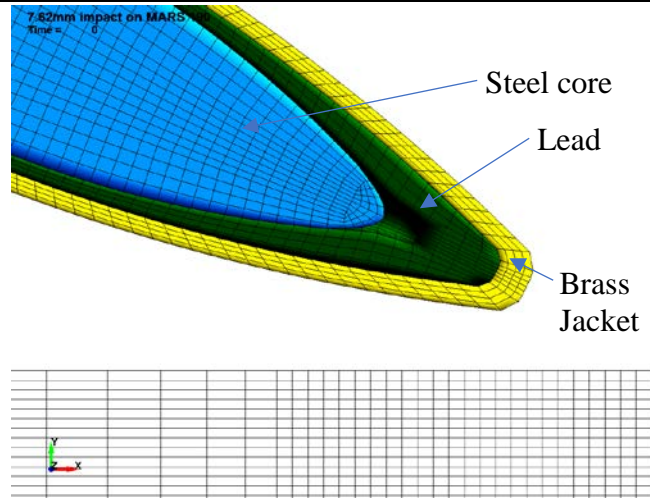


Figure 3: Discretization of the computational domain: (a) overview of whole domain (b) detail view and description of the different parts of the projectile.

Restricted by the computational resources and the demand to obtain results of several obliquity angles overnight, the following resolution is chosen:

The target is discretized with 32 elements in thickness direction and 80 elements in plane direction resulting in 204.800 elements in total. The refinement of the plane is concentrated in the middle where 64 x 64 elements are located leading to a spacing of 0.7 mm, the spacing in thickness direction is 0.25 mm. Our model does not exploit symmetry since the ricochet effect is fully three-dimensional.

The discretization of the projectile consists of the following parts: steel core, lead and jacket. In radial direction eight elements are used for the core and four for both - lead and jacket - and the longitudinal direction consists of 60 - 70 elements such that the spacing is also below 1 mm. In total, this leads to 12.544 elements for the core, 6.480 for the lead, and 6.336 elements for the jacket, and thus 25.360 elements for the whole projectile.

All parts are modeled with the Johnson-Cook material model which includes a dependency on strain, strain rate and temperature. Johnson and Cook express the flow stress as

$$\sigma_y = (A + B\bar{\epsilon}^n)(1 + c \ln \dot{\epsilon}^*)(1 - T^{*m}) \quad (1)$$

where  $A, B, C, n$ , and  $m$  are user defined input constants [1], and:

$\bar{\epsilon}^p$  = effective plastic strain,

$\dot{\epsilon}^* = \frac{\dot{\bar{\epsilon}}^p}{\dot{\epsilon}_0}$  = effective plastic strain rate for  $\dot{\epsilon}_0 = 1s^{-1}$ ,

$T^* = \frac{T-T_0}{T_m-T_0}$  = homologous temperature.

In the upper definitions  $\dot{\epsilon}_0$  describes the strain rate of the experiment,  $T_0$ , the temperature of the experiment and  $T_{melt}$  the melting point of the material under standard condition (i.p.  $p = 1bar$ ).

LS-DYNA conquers the nonlinearity in the dependence of flow stress on plastic strain by using a Taylor series expansion with linearization about the current time avoiding the necessity for iteration.

Further the Johnson-Cook fracture model is used, which estimates a fracture strain

$$\epsilon^f = [D_1 + D_2 \exp D_3 \sigma^*][1 + D_4 \ln \epsilon^*][1 + D_5 T^*], \quad (2)$$

where  $D_i, i = 1, \dots, 5$  are input constants and  $\sigma^*$  is the ratio of pressure divided by effective stress  $\sigma^* = \frac{p}{\sigma_{eff}}$ .

Fracture occurs when the damage parameter

$$D = \sum_{t_i} \frac{\Delta \bar{\epsilon}^p}{\epsilon^f} \quad (3)$$

reaches the value 1, where  $\epsilon^f$  is the material specific fracture parameter.

The JC-parameters for the present case are taken from literature: the MARS190® armor steel of the target plate is characterized by Gailly [2], the steel core is described by Favorsky [3], the lead is investigated by Adams [4] and the bronze of the jacket is characterized by Kilic [5]. The following table summarizes the utilized parameters:

Material	Elastic constants and density			Yield stress and strain hardening			Strain rate hardening	
	$G[MPa]$	$\nu$	$\rho \left[ \frac{kg}{m^3} \right]$	$A[MPa]$	$B[MPa]$	$n$	$\dot{\epsilon}_0 [s^{-1}]$	$C$
Target	79600	0.34	7850	844	1000	0.15	1e-3	0.01
Core	78400	0.34	7840	500	1000	0.2	1e-3	0.008
Lead	5600	0.34	11340	240	300	1.0	5e-4	0.1
Jacket	40000	0.34	8960	90	505	0.42	5e-4	0.01

Table 1: Material properties of all components and respective Johnson-Cook parameters.  $G$  is the Young's modulus,  $\nu$  the Poisson's ratio,  $\rho$  the density and the other parameters are defined in the description of the JC-model.

Material	Adiabatic heating and temperature softening				Fracture strain constants				
	$c_p \left[ \frac{J}{kgK} \right]$	$T_m[K]$	$T_0[K]$	$m$	$D_1$ brittle	$D_2$	$D_3$	$D_4$	$D_5$ temp
Target	450	1800	293	1.058	0.00	2.12	-1.45	0.00	-0.68
Core	475	1800	293	1	0.00	0.00	0.00	0.00	0.00
Lead	129	327.5	293	1	0.3	0.00	0.00	0.00	0.00
Jacket	386	1356	293	1.68	0.54	4.89	-3.03	0.014	1.12

Table 2: Fracture relevant material parameters and fracture strain constants for the Johnson-Cook fracture model (compare Equations (1) and (2)), plus the heat capacity coefficient  $c_p$ .

Material	Grüneisen Parameters			
	$C_0 \left[ \frac{m}{s} \right]$	$S_1$	$\gamma_0$	$a$
Target	4570	1.4	1.97	0
Core	4700	1.29	1.587	0
Lead	2028	1.627	2.253	0
Jacket	3720	1.328	1.657	0

Table 3: Equation of state: Grüneisen parameters for investigated materials.

Only brittle fracture is assumed for lead and core since no fracture material data are available. This is achieved by setting only the  $D_1$  parameter and leaving all other fracture parameters at the default value (0.0). Since significant negative contact energy is observed for the core if the proposed value of  $D_1 = 0.5$  is used, instead this value is set to 0.0 which causes LS-DYNA to only erode elements that are no longer computable due to aspect ratio or skewness. This is consistent with the approach used in the previous paper of Seidl [1]. The

melting temperature and Young's modulus of the lead is significantly lower compared to the other materials, while the properties of the other materials are rather similar.

In cases of high strain rates, an equation of state is required to account for the influence of internal energy and density on the pressure and vice versa. Typically, the Mie-Grüneisen equation is used to determine the pressure state of shocked solids [6]. The general expression is:

$$P - P_H = \frac{\gamma}{v} (E - E_H) \quad (4)$$

with reference state H (one point on the Hugoniot) and the Grüneisen parameter  $\gamma$ . An often used approximation is that the ratio  $\frac{\gamma}{v} = \frac{\gamma_0}{v_0}$  is constant. The variant implemented in LS-DYNA reads

$$P(\mu, E) = \frac{\rho_0 C_0^2 \mu \left[ 1 + \left( 1 - \frac{\gamma_0}{2} \right) \mu - \frac{a}{2} \mu^2 \right]}{\left[ 1 - (S_1 - 1) \mu - S_2 \frac{\mu^2}{1 + \mu} - \frac{S_3 \mu^3}{(1 + \mu)^2} \right]^2} + (\gamma_0 + a\mu) E \quad (5)$$

where  $\rho_0$  is the solid density,  $C_0$  is the elastic sound speed,  $\gamma_0$  is the Grüneisen parameter,  $a$  is the first order volume correction to  $\gamma_0$  and the coefficients  $S_i$  define the cubic  $U_S$  to  $u_P$  relationship. The corresponding values for the materials of each part are listed in **Fehler! Verweisquelle konnte nicht gefunden werden.**  $S_2$  and  $S_3$  are not available for any of these materials and thus not listed here.

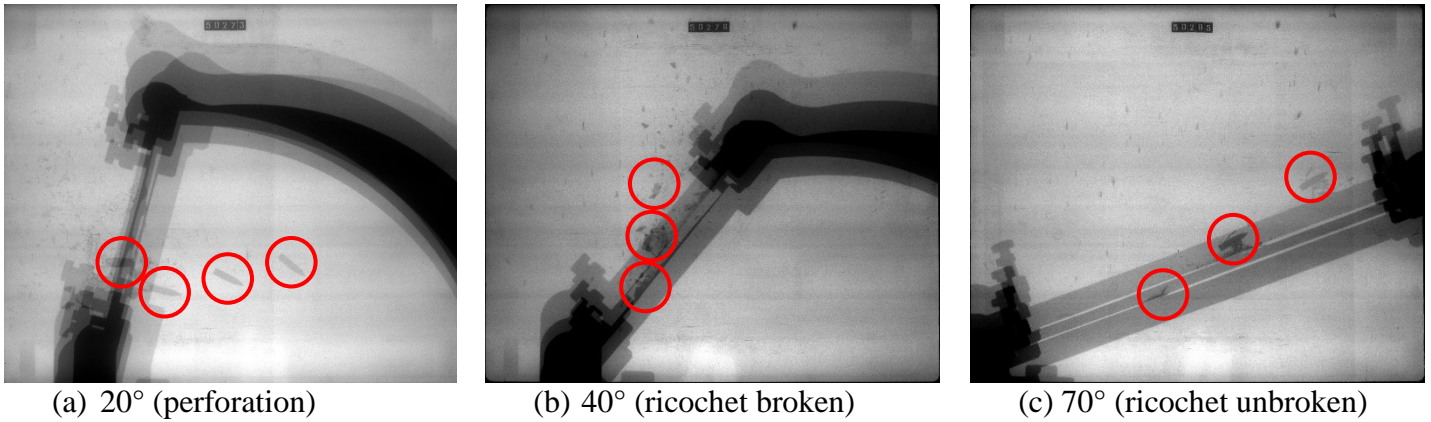


Figure 4: Experimental results: Quad and triple exposed x-ray images of impact with 100 $\mu$ s delay.

## 4. Results and Discussion

This section compares the experimental and numerical results for the impact of an armor-piercing projectile on an inclined plate, as extensively described in section two and three, for oblique angles between  $0^\circ \leq \theta \leq 70^\circ$ . The simulations are set up with an angular resolution of  $\Delta\theta = 2^\circ$  while the experiments are conducted in  $10^\circ$  steps. Due to the chaotic behavior of break-up and fragmentation of the projectile three shots are investigated at each angular position. Images where the projectile parts could not be identified with certainty are not considered in the evaluation.

In the numerical simulation, the influence of the jacket and lead is investigated in addition, executing one family of simulations considering all parts of the projectile (“full-projectile”) and one considering only the core (“core-only”).

For simplification, three main scenarios can be distinguished (cp. Figure 4): perforation of the target ( $0^\circ \leq \theta \leq 30^\circ$ ), broken ricochets ( $30^\circ < \theta \leq 60^\circ$ ) and unbroken ricochets ( $60^\circ < \theta \leq 70^\circ$ ). To cover the whole range in the comparison the angles 20, 40 and 70 degrees are further investigated in the following discussion.

First, the 3D numerical results of the full projectile for the addressed angles are presented, then the residual velocity, i.e. the projectile's velocity after the impact, the eroded mass and the deflection angle are investigated with respect to the oblique angle. Next, a more detailed investigation of the evolution of deflection angle and

residual velocity is presented for the three representative angles. Finally, the damage at the target is compared qualitatively.

In Figure 5, a symmetrically sliced half-plane of the numerical results is shown at four time steps and for the three representative oblique angles. Figures (a) - (d) show the perforation scenario for the oblique angle of 20°. While the lead and the jacket are nearly completely eroded, the projectile is only slightly affected and is only little deflected. The damage of the target is considerably larger in diameter than the diameter of the metal core and thus considerable differences between simulating the full projectile and the core are expected for the perforation scenario.

For the case of  $\theta = 40^\circ$ , where the experiment reveals fragmentation of the core (cp. Figure 4 (b)), the lead and the jacket are again nearly completely destroyed. The projectile erodes a significant amount of material from the target but still ricochets. The last image is captured after a twice as long time-span compared to 20° and 70° since the interaction between threat and target is considerably longer.

Figures (i)-(l) show the case of  $\theta = 70^\circ$  where in the experiment unbroken ricochet is observed (cp. Figure 4 (c)). Here, the core remains rather unaffected and also little perforation is observed at the projectile, while the jacket is broken - but not completely eroded.

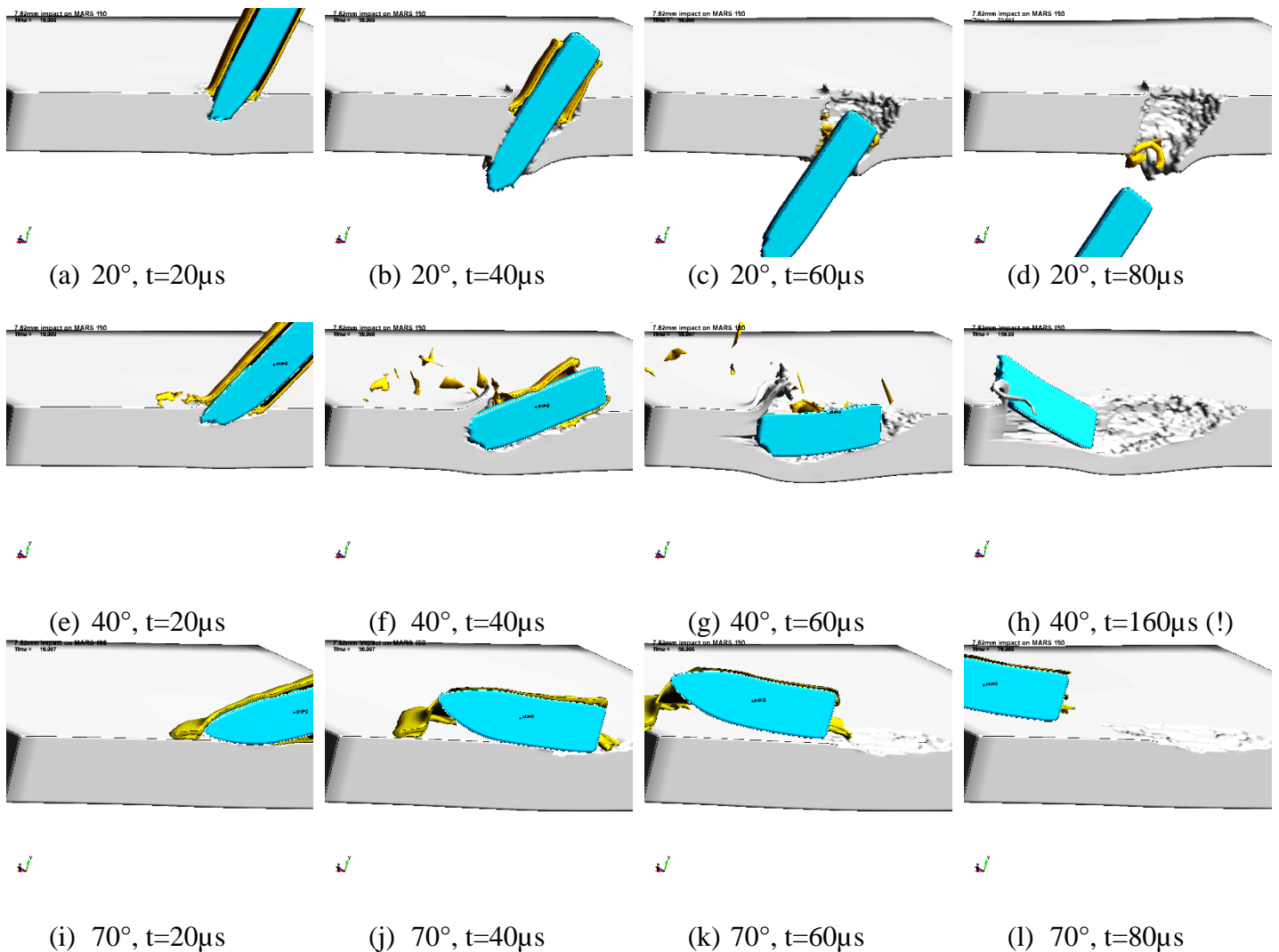


Figure 5: Slices of numerical results for impact (first row), transition (second row) and ricochet case (third row) at four time steps of 20, 40, 60 and 80 microseconds.

In the following plots, the blue line color indicates the results where only the core is modeled, the orange color depicts the numerical results of the full projectile, and the experimental results are visualized in red color.

Figure 6 shows the residual velocity of the projectile over the oblique angle. The numerical results of both modeling techniques show a similar trend. In the region where the threat penetrates the target the residual velocity decreases with increasing oblique angle while the opposite is observed for the ricochet case. Considering first the perforation case, the simulations with the full-projectile predict a higher residual velocity than the “core-only” simulation which corresponds up to 15° oblique angle better to the experimental results. However, the “core-only” simulation predicts the critical angle between penetration and ricochet more accurate. In the region of more than fifty degrees the differences between both modelling techniques and the experimental results are acceptably small and there is no need to simulate the whole projectile. Concerning residual velocity, the results are also promising in the region where fracture was observed in the experiment, although fracture was not modeled in the simulation.

Comparing the velocity components illustrated in the right subfigure it shows that the tangential velocity component is nearly identical for  $0^\circ \leq \theta \leq 20^\circ$  and  $55^\circ \leq \theta \leq 70^\circ$ , while the normal velocity only matches for angles between  $45^\circ \leq \theta \leq 70^\circ$ . Thus, for low angle impact only the normal velocity component is affected. Figure 7 compares the eroded mass of the target and the angular deflection – both properties which are of huge interest when designing armor or predicting the ballistic trajectory of the ricochet.

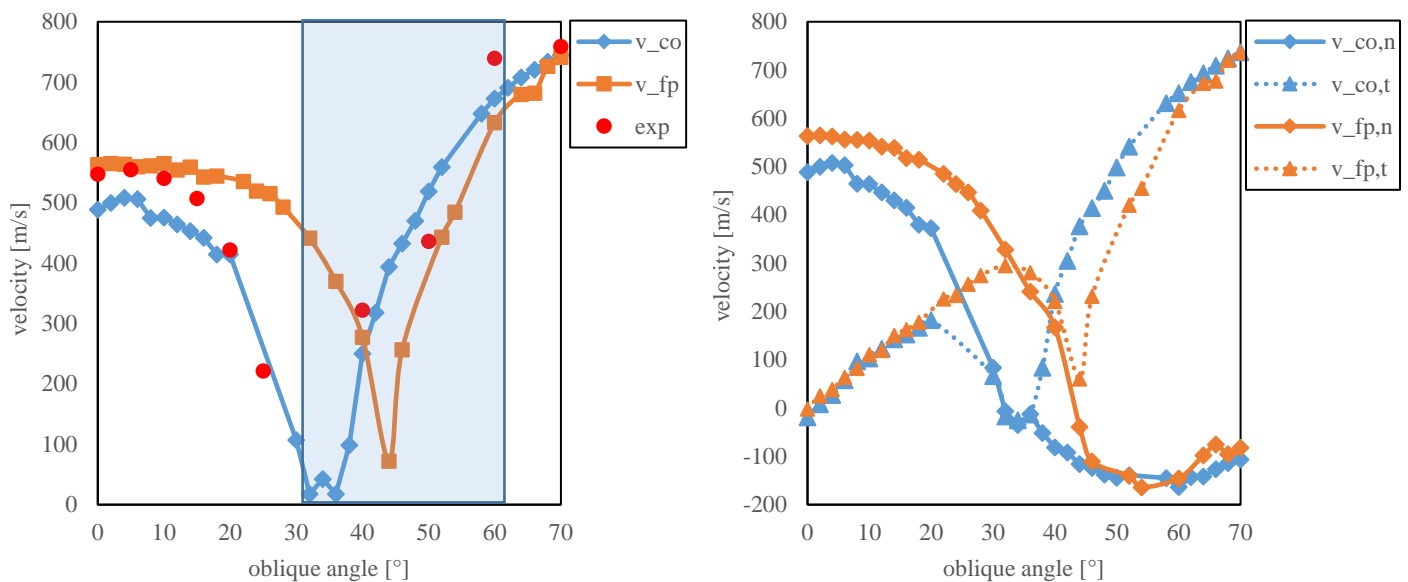


Figure 6: Residual velocity and velocity of ricochet for numerical simulations of “full-projectile” (orange) and “core-only” (blue). Absolute values are depicted in the subfigure on the left and the subdivision into normal- and tangential-component is shown in the right subfigure. Values where projectile breaks (oblique angle between 30 and 60 degrees) have to be regarded with caution. (fp = “full projectile”, co = “core only”)

Considering the eroded mass of the target, massive differences are found when comparing the “full-projectile” with the “core-only” simulation. One reason for this is the significant mass of lead and jacket due to which the “full-projectile” is more than three times as heavy as the core and thus has also three times as much kinetic energy. Further, the total kinetic energy of the hull is transformed into erosion and deformation of hull and target, while the “core-only” loses a part of its kinetic energy. While the eroded mass increases for oblique impact up to the critical ricochet angle in the simulation, the experiment predicts the opposite. As discussed later, this phenomenon might be since less plugging happens for oblique impact. If the oblique angle is larger than  $50^\circ$ , less mass is eroded compared to the perpendicular impact.

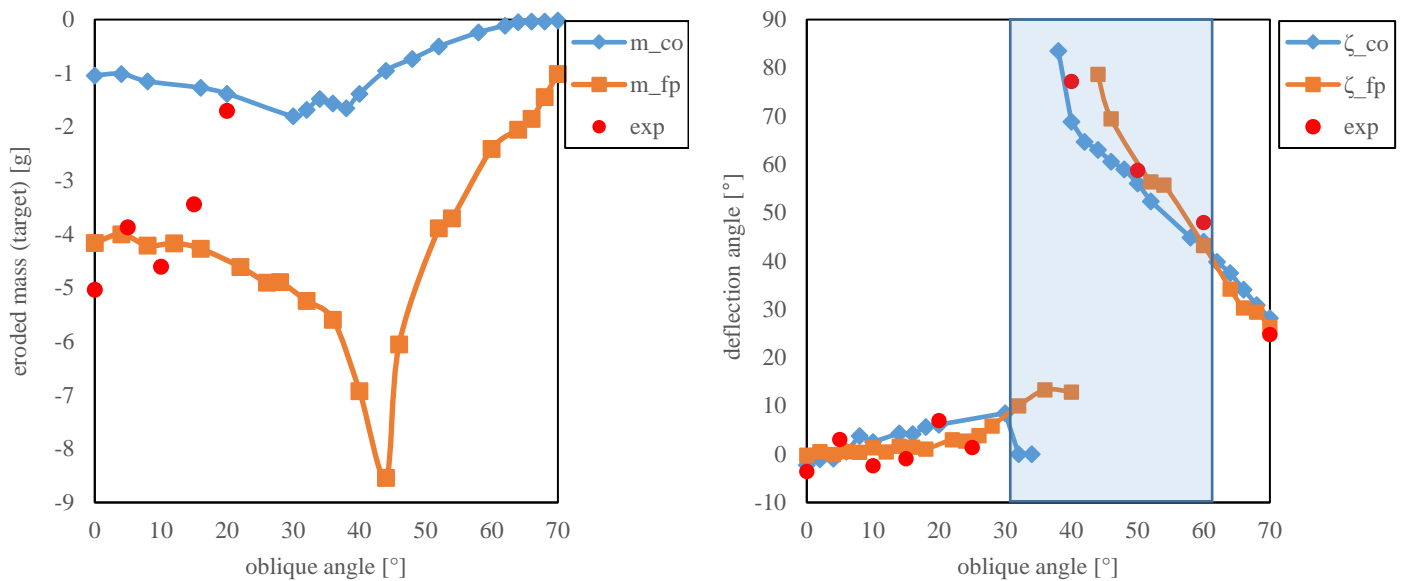


Figure 7: Eroded mass of target and angular deflection of projectile. Values where projectile breaks (oblique angle between 30 and 60 degrees) have to be regarded with caution. (fp = “full projectile”, co = “core only”).

The deflection angle indicates for the perforation case whether the core is deflected or goes straight through the material, and for the ricochet case it measures how close the ricochet is to an ideal elastic impact.

While the deflection angle of the simulation of the whole projectile is close to zero up to 20° of oblique angle, a steady increasing deflection is observed for the “core-only” simulation. The experiment predicts also a very small deflection angle with an average standard deviation of 4.2 degree, which however might also be due to slightly yawed impact.

For the ricochet case, the deflection angle of both simulations and the experiment match very well.

In Figure 8, the residual velocity and the deflection angle are shown over the simulation time. Since it is not possible to use a high speed camera for observation of ricochet experiments, this quantity can not be extracted from experiment and thus only the two modelling techniques can be compared. This motivates further development in numerical simulation since it offers a possibility to gain a deeper insight in physics, which is not accessible with experimental techniques.

The legend depicted on the right relates to both subfigures, and uses the same color convention as before (e.g., “p\_20” stands for “full-projectile” against 20° inclined plate). The first subfigure shows the residual velocity. Since, according to Newton’s second law of motion, the resulting force is proportional to the change in momentum, the force acting on the projectile and also on the target can be directly derived from the steepness of the velocity curves. Further, the end of interaction can be determined by the time where the acceleration remains zero. Since the critical angle predicted for the two approaches differs, the curves corresponding to the inclined plate at 40° can not be compared against each other but only against the results for different oblique angles of the same modeling technique. By accident, these curves match quite well (fp-40 and co-40). The steepness of the curves of 20° and 40° are similar up to 30 μs for both “full-projectile” and “core-only” result while the steepness of the “full-projectile” is slightly larger in magnitude. For impact under an oblique angle of 70° both simulations predict a similar behavior.

The subfigure on the right shows the deflection angle shifted by the ricochet angle for a clearer plot. While for the impact under an oblique angle of 20° the “full-projectile” is only little deflected, considerable deflection can be observed between 25 μs and 60 μs (up to 12.6° deflection). After 60 μs both simulations have a similar deflection (“core-only” 5.6°, “full-projectile” 3.1°).

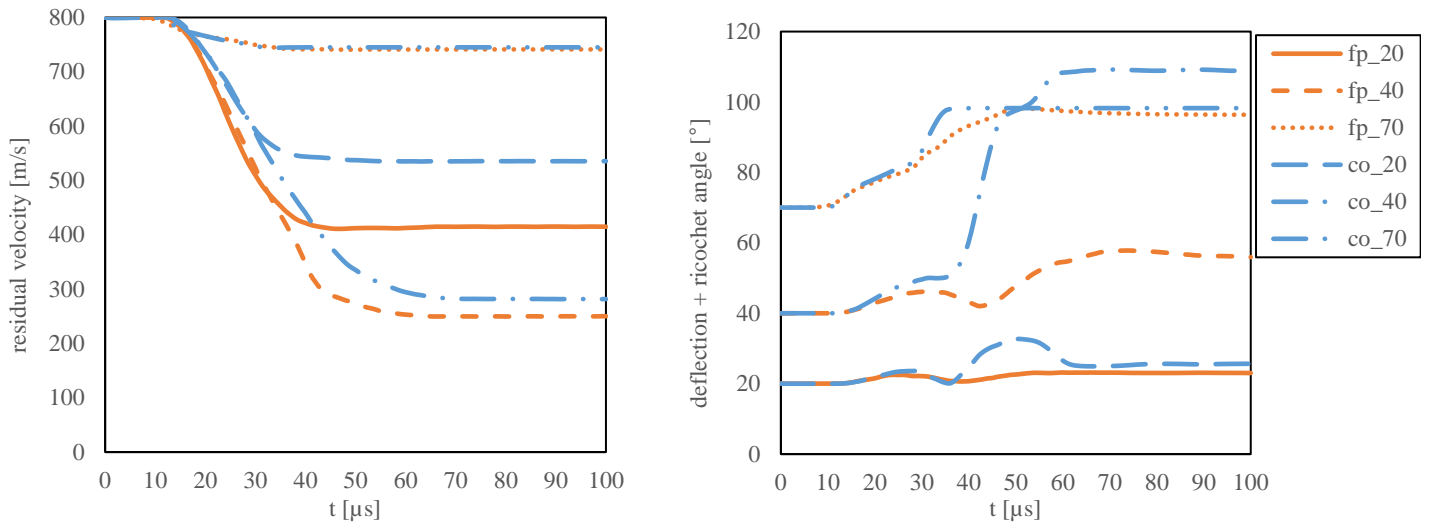


Figure 8: Residual velocity and deflection angle as a function of simulation time. The legend on the right describes both subfigures (fp = “full projectile”, co = “core only”)

For the case of 40°, the “full-projectile” shows a similar behavior to the “core-only” shape of  $\theta = 20^\circ$ , while the steep increase in deflection for the “core-only” results of 40° indicate the ricochet of the core. The shape for  $\theta = 70^\circ$  are similar in curve shape and resulting deflection angle, which underlines the hypothesis found previously that for ricochet, the consideration of the lead and jacket is not necessarily required.

The next two figures investigate the deformation at the target for both modeling techniques and the experiment. Figure 9 shows the half plane of the sliced target plate for impact under an oblique angle of 20° where perforation is observed for all settings. Clearly, the largest diameter of the bullet hole inlet is observed in the experiment (16.3 mm) compared to “full-projectile” (13.3 mm) and “core-only” simulation (8.1 mm). While the numerical results of the “full-projectile” still predict a considerably large diameter after the impact (8 mm) compared to the diameter of the core (5.8 mm), the “core-only” simulation predicts 6.2 mm, and in the experiment 6.5 mm are observed. Further, a much more ductile material behavior of the target is observed in the experiment than predicted with the numerical simulation. The bending of the plate is much more distinct in the experiment which might be the reason for the opposite behavior in the eroded mass measured in the experiment (cp. Figure 7). It’s unclear whether these differences arise due to the erosion of deformed elements in the simulation and could be conquered by an ALE or a SPH approach, the refinement of the grid itself, or an unsuited material model.

Figure 9 compares the depth and length of the impact between both modeling techniques for an impact under 70° oblique angle. For the “full-projectile” a distinct amount of erosion at the metal-plate is observed (1.1 g)

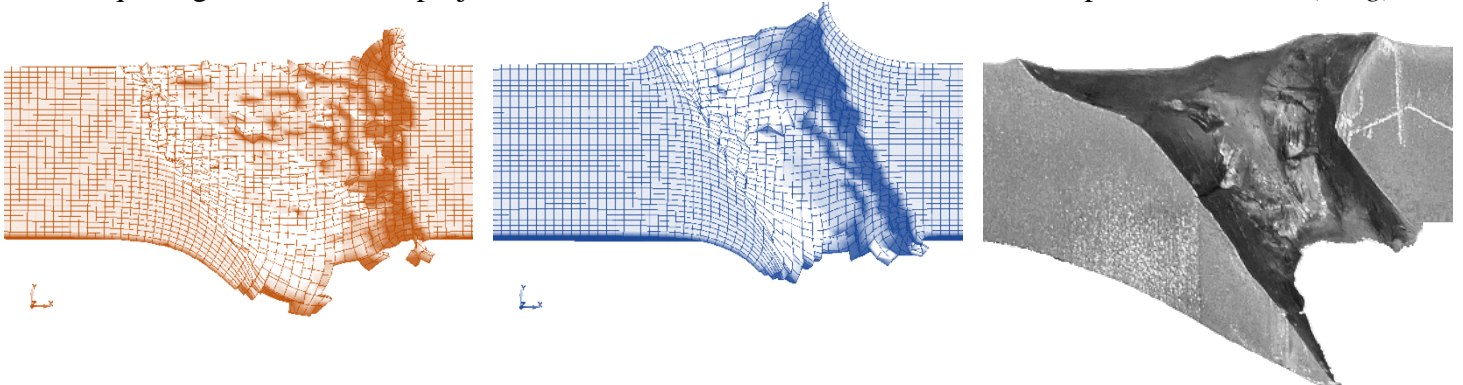


Figure 9: Eroded elements of target for oblique impact of 20 degrees. Comparison between “full-projectile” (left) and “core-only” (middle) and experiment (right).

and the length of the well is also pronounced ( $23\text{ mm}$ ). On the other hand, the “core-only” simulation predicts minor erosion ( $0.014\text{ g}$ ) and also a smaller length of the well ( $17\text{ mm}$ ). Further, the point of maximum depth of ( $-0.9\text{ mm}$ ) is measured  $9\text{ mm}$  upstream of the point of maximum depth of the “full-projectile” ( $-0.7\text{ mm}$ ). The data measured in the experiment (length of  $16\text{ mm}$ ) correlate better with the results of the simulation where only the core is modeled.

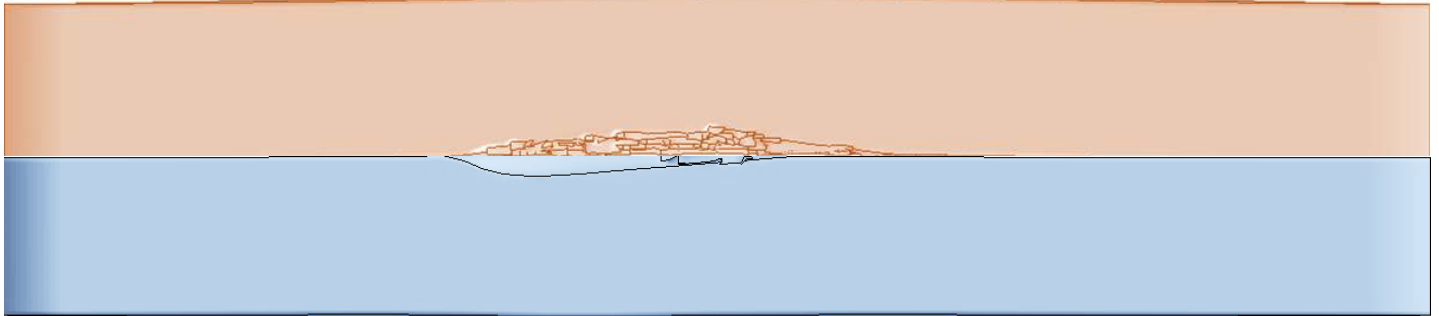


Figure 10: Eroded elements of target for oblique impact of 70 degrees. Comparison between “full-projectile” (upper image) and “core-only” (lower image).

## 5. Outlook

To conquer the issue, discussed in this paper, that core failure can not be reproduced with the classical FEM-approach following studies will evaluate the possibilities of the SPH (smooth particle hydrodynamics) formulation. In a first step, a proper particle distribution has been set up for a more simple case of a projectile surrogate, first simulations are conducted and a python post-processing algorithm to detect the resulting fragments has been developed (compare Figure 11). Further experiments have to be performed to evaluate the accuracy of SPH and determine the most suitable particle distribution and SPH-formulation for this application.

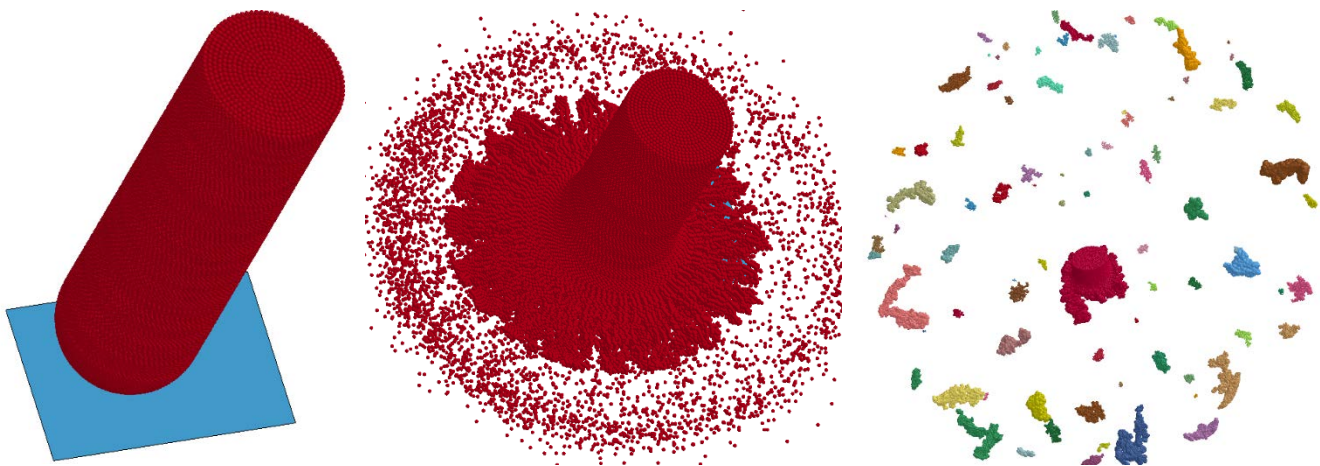


Figure 11: Outlook and first results: SPH particle configuration (left), mushrooming briefly after impact (middle), fragment detection at the end of the simulation (right).

## 6. Conclusion

This paper investigates the full range of oblique impact at a fixed velocity of  $800\text{ m/s}$  for a  $7.62\text{ mm}$  projectile. Besides the commonly used validation parameter  $v_{res}$ , the eroded mass of the target and also the deflection angle of the projectile were investigated. Further, the influence of considering jacket and lead were studied. It was shown that jacket and lead had a distinct influence on the simulation results. The residual velocity was only similar for oblique angles greater  $60^\circ$  and the eroded mass was four times larger when considering the hull. However, the deflection angle deviated only little except for the region around the critical angle. Compared with the experiment, the residual velocity is well predicted by the simulation of the full projectile. Accordance between the deflection angles could only be found for the ricochet case. Although no fracture could be applied, these quantities could be reproduced with the simulation independent of whether the core fractured in the experiment or not.

Although the experimental results could be partly reproduced, the aim is to have a better characterization of the threat, which also predicts the fracture of the core. With the decent possibilities of LS-DYNA this is not possible and further the failure of the core had to be modified. An improved implementation would help to develop protection which exploits the knowledge by means of favoring core-break and thus reducing the danger of ricochet.

## References

- [1] M. Seidl, T. Wolf and R. Nuesing, "Numerical Investigations on Ricochet of a Spin-Stabalised Projectile on Armour Steel Plates," in *11th European LS-DYNA Conference 2017*, Salzburg, Austria, 2017.
- [2] B. Gailly, *Etude du Comportement Dynamique et de la Rupture de Trois Aciers a Blindage*, Paris, 1996.
- [3] V. Favorsky et al., *Experimental-Numerical Study of Inclined Impact in Al7075-T7351 Targets by 0.3" AP Projectiles*, US: 26th ISB, 2011.
- [4] B. Adams, *Simulation of Ballistic Impacts on Armored Civil Vehicles*, Eindhoven, 2006.
- [5] N. Kilic and S. Bedir, "Ballistic behavior of high hardness perforated armor plates against 7.62 mm armor piercing projectile," *Materials and Design*, 2014.
- [6] M. Scapin, *Shock-wave and high strain-rate phenomena in matter: modeling and applications*, Turin: Politecnico di Torino, 2013.